

The Influence of Poly(phenyleneethynylene) Side Chain Structure on Single-Walled Carbon Nanotubes Hybrid Photovoltaic Cells

Jie Mao¹, Qian Liu², Shujing Wang¹, Xin Lv¹, Yi Huang¹, Yanfeng Ma¹,
Yongsheng Chen^{1,*}, and Shougen Yin^{2,*}

¹Key Laboratory for Functional Polymer Materials and Center for Nanoscale Science and Technology,
Institute of Polymer Chemistry, College of Chemistry, Nankai University, Tianjin 300071, China

²Institute of Material Physics, Tianjin University of Technology and
Tianjin Key Laboratory for Photoelectric Materials and Devices, Tianjin 300384, China

Delivered by Ingenta to:

A novel poly(phenyleneethynylene)/single walled carbon nanotubes (SWNTs) donor-acceptor nanohybrid system was constructed based on the bulk heterojunction concept, and their photovoltaic (PV) properties were studied. Comparing with that of the pristine polymer poly(phenyleneethynylene) (PPE) device, the PV performance of the SWNTs/PPE hybrid is dramatically improved. The origin of open-circuit voltage (V_{oc}) of the pristine polymer PPE device and SWNTs/PPE device was explained by metal-insulator-metal (MIM) diode model and pinning mechanism, respectively. Furthermore, incorporation of sensitizing groups to the side chain of PPE has great effect on the photovoltaic cell performance based on these hybrid materials and both the short-circuit current density (I_{sc}) and power conversion efficiency are significantly enhanced. It is proposed that the main reason for the increase of short circuit current is due to efficient transfer of holes by sensitizer to PPE backbone and the transfer of electrons to the SWNTs. The power conversion efficiency is enhanced by ~ 1 order magnitude to 0.031% for the device based on the PPE3 with anthracene sensitizer group on the side chain compared with that ($4.2 \times 10^{-3}\%$ for SWNTs/PPE1 and $6.2 \times 10^{-3}\%$ for SWNTs/PPE2) of the device without anthracene sensitizer on the side chain.

Keywords: Single Walled Carbon Nanotubes, Poly(phenyleneethynylene), Synthesis, Sensitizer, Photovoltaic Cell.

1. INTRODUCTION

Polymer solar cells (PSC) have attracted great interest due to their mechanical flexibility, lightweight, and potential low cost of fabrication of large areas.^{1–5} During the past decade, efficient photovoltaic systems based on interpenetrating network of π -conjugated polymer donor and fullerenes acceptor using the bulk heterojunction structure have been a focus of intensive research efforts.^{5,6} Fullerene compounds (e.g., PCBM) have been considered one of the best π -electron acceptors and various electron-donating materials has been studied with these electron-accepting materials.^{2,3,5} Considered as the longest fullerene molecule, carbon nanotubes have been used recently as the electron-accepting materials for photovoltaic devices.^{7–13} Comparing with C_{60} , single

walled carbon nanotubes (SWNTs) have many advantages including their huge π - π conjugation, high charge mobility and one-dimensional structure. The large surface area of SWNTs would allow intrinsically formation of high interfacial heterojunction area between nanotubes and the conjugated polymer chains, potentially creating large dissociation regions and enhancing the PV performance. Indeed, recent results from Kymakis et al.^{7–9,13} and others^{11,12,14} as well as ours¹⁰ indicated that the SWNTs/polymer hybrid systems exhibited enhanced photoactive properties comparing with polymer matrix itself.

Poly(phenyleneethynylene)s (PPEs), a kind of rigid-rod π -conjugated polymer, are of great interest because of their semiconductor-like properties and ease of processing, which makes them fulfill the requirements for many potential applications especially for electronic and photonic devices.¹⁵ Recent researches reveal that adding SWNTs into the polymer solution can quench the

*Authors to whom correspondence should be addressed.

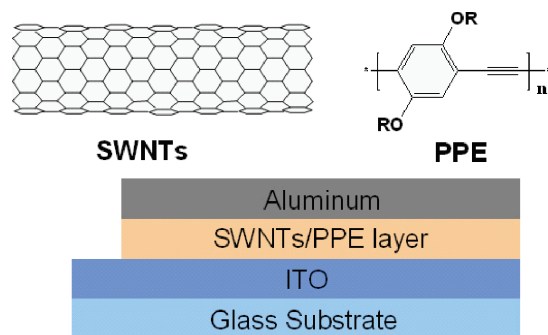


Fig. 1. A schematic device structure based on SWNTs/PPE hybrid materials, together with chemical structure of the materials used for the active layer.

fluorescence of excited PPE.^{10,16} Quenching is believed to occur via photoinduced electron transfer mechanism, where the photoexcited PPE serves as the electron donor and the SWNTs act as the electron acceptor. This finding suggests that PPE/SWNTs hybrid systems may be used to build PV devices where exciton split occurs at the nanoscale heterojunction between PPE and SWNTs, leading to the efficient production of charge carriers.

Continuing our recent investigation for PPE/SWNTs PV studies,¹⁰ in this paper, we used different side chain functionalized PPEs to hybridize SWNTs and examined their photovoltaic properties based on the bulk heterojunction concept (Fig. 1). The results show that the heterojunction is formed in the system between SWNTs and the PPE polymer, which dramatically improve photovoltaic performance of the polymer devices. Furthermore, with better light absorbing sensitizer groups on the PPE side chains, the photovoltaic performance is further significantly enhanced.

2. EXPERIMENTAL DETAILS

2.1. Instruments and Measurements

UV-Vis-NIR spectra were obtained with a JASCO V-570 spectrometer. ¹H NMR spectra were recorded on a Bruker (300 MHz) spectrometer using TMS as the internal standard. Gel permeation chromatography (GPC) analysis was conducted on a Waters 510 system using polystyrene as the standard and THF as eluent at a flow rate of 1.0 mL min⁻¹ at 40 °C. The electrochemical cyclic voltammetry (CV) was conducted on Ecochemie μ Autolab III electrochemical station employing a Pt disk as the working electrode, Ag/Ag⁺ electrode (0.01 M AgNO₃) as the reference electrode, and a Pt wire as the counter electrode. The reference electrode was calibrated with ferrocene ($E_{\text{Fc}/\text{Fc}^+} = 0.07$ V vs. Ag/Ag⁺). Tetrabutylammonium perchlorate (TBAP) was the supporting electrolyte, and the scan rate was 50 mV s⁻¹. Transmission electron microscope (TEM) images were obtained on a FEI TECNAI-20 instrument operated at 200 kV. Sample preparation involved

sonicating purified SWNTs in DMF for 1 h and dropping the resulting suspension onto carbon-coated copper grids. Raman spectra were measured by a Renishaw in Via Raman microscope at room temperature with the 514.5 nm line of an Ar ion laser as the excitation source. Centrifugation was carried out with an Eppendorf 5810R centrifuge. The current–voltage (I – V) measurement of the photovoltaic devices was conducted on a computer controlled Keithley 2400 Source Measure Unit. A Xenon lamp with AM 1.5 filter was used as the white light source, and the optical power at the sample was 100 mW cm⁻² through the glass/ITO side. The calculation of the power conversion efficiency, η , has been performed using the equation:

$$\eta = \frac{FF \times I_{\text{sc}} (\text{A/cm}^2) \times V_{\text{oc}} (\text{V})}{P_{\text{in}} (\text{W/cm}^2)} \quad (1)$$

where V_{oc} , I_{sc} , FF , and P_{in} are the open circuit voltage, the short circuit current, the fill factor and the incident light power, respectively. The fill factor (FF) is determined according to $FF = (V_{\text{m}} I_{\text{m}})/(V_{\text{oc}} I_{\text{sc}})$, where V_{m} and I_{m} are the voltage and the current in the maximum power point of the I – V curve in the fourth quadrant.

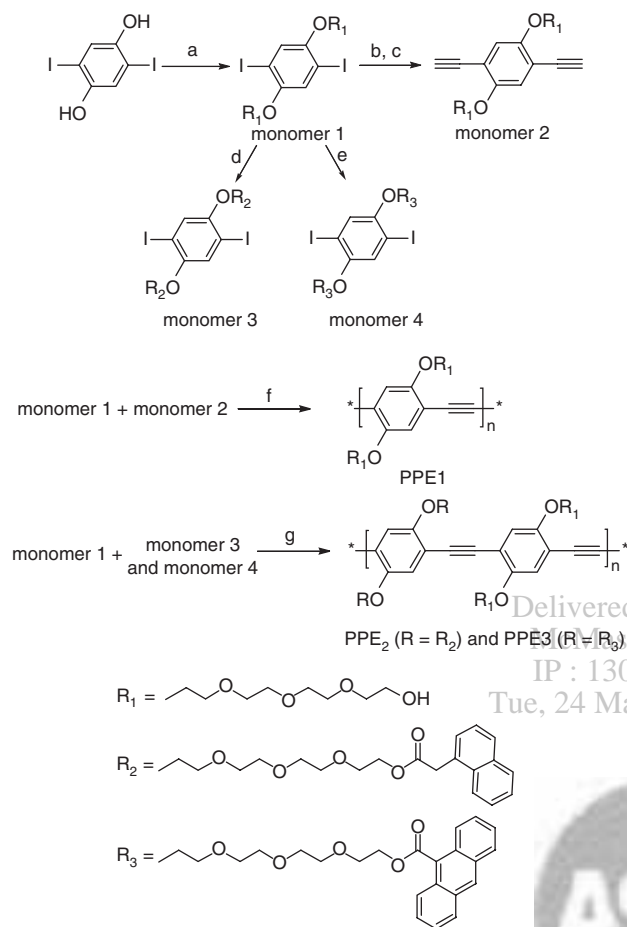
2.2. Materials

The SWNTs were prepared in our lab using a modified direct current arc-discharge method.¹⁷ All chemical reagents used in this study were purchased from commercial sources (Alfa, Acros and Aldrich). Toluene and THF were purified by distillation from sodium in the presence of benzophenone. Other organic solvents were used without any further purification. 1,4-Diiodo-2,5-bis(11-hydroxyl-3,6,9-trioxaundecyl)benzene (monomer 1, see Scheme 1 below) was synthesized according to the literature procedures,¹⁸ 1,4-Diethynyl-2,5-bis(11-hydroxy-3,6,9-trioxaundecyl)benzene (monomer 2) and Poly((2,5-bis(11-hydroxy-3,6,9-trioxaundecyl)-*p*-phenylene) ethynylene) (PPE1) were synthesized according to our procedures reported earlier.¹⁰ All reactions were carried under argon if not stated otherwise. Indium tin oxide (ITO) coated glass, $R_s = 10 \Omega$ square⁻¹, was purchased from CSG Inc.

2.3. Synthesis

Conditions:

- 11-Hydroxy-3,6,9-trioxaundecyl-1-*p*-toluenesulfonate, K₂CO₃, acetone, DMF, reflux, overnight, 50%.
- Me₃SiC≡CH (TMSA), Pd(PPh₃)₂Cl₂, CuI, *i*-Pr₂NH (DIPA), toluene, 60 °C, 22 h, 96%.
- KOH, MeOH-THF, 25 °C, 48 h, 83%.
- 1-naphthylacetyl chloride, Et₃N, CHCl₃, 70 °C, 20 h, 90%.
- 9-anthracenecarbonyl chloride, Et₃N, CHCl₃, 70 °C, 20 h, 92%.
- Pd(PPh₃)₄, CuI, *i*-Pr₂NH, Toluene, 60 °C, 60 h, 91%.
- Pd(PPh₃)₄, CuI, *i*-Pr₂NH, THF, 60 °C, 60 h.



Scheme 1. Synthetic route of the monomers and polymers.

1,4-Diiodo-2,5-bis(11-(1'-naphthylacetyl)ate)-3,6,9-trioxaundecyl)benzene (monomer 3) and 1,4-Diiodo-2,5-bis(11-(9'-anthracenecarboxylate)-3,6,9-trioxaundecyl)benzene (monomer 4): 1-Naphthaleneacetic acid (1.12 g, 6 mmol) was converted to the corresponding acid chloride by treating with SOCl_2 . A 10 mL aliquot of SOCl_2 was placed in an N_2 -purged flask followed by the addition of 1.12 g of 1-Naphthaleneacetic acid and one drop of anhydrous DMF was added as the catalyst. After the mixture was stirred at 80 °C for 7 h, excess SOCl_2 was removed under distillation. Then dried toluene (10 mL) was added, the mixture was heated up and the SOCl_2 /toluene azeotrope was distilled out. This procedure was repeated three times to ensure removing SOCl_2 completely. Finally, the product (1-naphthylacetyl chloride) was dried under vacuum and used for the following step.

To a solution of monomer 1 (0.71 g, 1 mmol) and freshly prepared 1-naphthylacetyl chloride (6 mmol) above in dry chloroform (100 mL) was added triethylamine (5.6 mL, 20 mmol). The reaction mixture was stirred at 70 °C for 20 h. After completion of the reaction, the mixture was cooled to room temperature and evaporated to dryness under reduced pressure, and then diluted with

100 mL ethyl acetate. The organic salt was filtrated off and washed with ethyl acetate (20 mL \times 2), then the combined filtrate was washed with brine (50 mL \times 3), dried over anhydrous Na_2SO_4 . The solvent was removed to yield the crude product, which was purified by column chromatography on silica gel with ethyl acetate/hexane (1/1) as eluant to give product monomer 3 (0.95 g, 0.9 mmol, 90%). $^1\text{H NMR}$ (300 MHz, CDCl_3 , δ/ppm): 3.64 (br t, 8H), 3.74 (br t, 4H), 3.84 (br t, 4H), 4.10 (m, 8H), 4.25 (br s, 4H), 6.97 (s, 2H), 7.41–7.55 (m, 8H), 7.78 (t, 2H), 7.85 (d, 2H), 7.99 (d, 2H). ESI-MS: 1073.2 ($\text{M} + \text{Na}^+$).

1,4-Diiodo-2,5-bis(11-(9'-anthracenecarboxylate)-3,6,9-trioxaundecyl)benzene (monomer 4, 1.03 g, 0.92 mmol, 92%) was synthesized following the same procedure as monomer 3. $^1\text{H NMR}$ (300 MHz, CDCl_3 , δ/ppm): 3.66–3.71 (m, 16H), 3.79 (t, 4H), 3.93 (t, 4H), 4.03 (t, 4H), 4.77 (t, 4H), 6.88 (s, 2H), 7.50 (m, 8H), 8.01 (d, 4H), 8.12 (d, 4H), 8.52 (s, 2H). ESI-MS: 1145.2 ($\text{M} + \text{Na}^+$).

Poly[2,5-bis(11-hydroxy-3,6,9-trioxaundecyl)-1,4-diethynyl-phenylene-*alt*-2,5-bis(11-(1'-naphthylacetyl)ate)-3,6,9-trioxaundecyl)-1,4-phenylene] (PPE2) and Poly[2,5-bis(11-hydroxy-3,6,9-trioxaundecyl)-1,4-diethynyl-phenylene-*alt*-2,5-bis(11-(9'-anthracenecarboxylate)-3,6,9-trioxaundecyl)-1,4-phenylene] (PPE3):

A 50 mL Schlenk flask equipped with a stir bar was charged with 1,4-Diethynyl-2,5-bis(11-hydroxy-3,6,9-trioxaundecyl)benzene (monomer 1, 214 mg, 0.42 mmol, 1.05 eq) and monomer 3 (420 mg, 0.40 mmol, 1 eq). Tetrakis-(triphenyl-phosphine)palladium (0) (23 mg, 20 μmol , 0.05 eq) and copper (I) iodide (7.6 mg) were added to the flask under an argon atmosphere. The flask was degassed by three freeze-pump-thaw cycles after adding THF (20 mL) and DIPA (2 mL) via a syringe needle and the reaction was stirred at 60 °C for 60 h. The crude product (460 mg, 91%) was precipitated out by pouring the reaction solution into 100 mL cold methanol. The collected product was then re-dissolved in 50 mL chloroform, washed with 0.1 M ammonium hydroxide (50 mL \times 2) and distilled water (50 mL \times 2), dried over anhydrous sodium sulfate. The solvent was then evaporated to yield the product PPE2, which was dried under vacuum as an orange solid. $^1\text{H NMR}$ (300 MHz, CDCl_3 , δ/ppm): 3.58–3.82 (br, m, 46H), 4.06–4.20 (br, m, 22H), 6.96–7.03 (br, m, 4H), 7.39–7.48 (m, 8H), 7.76–7.83 (br, m, 4H), 7.96 (br, d, 2H). GPC (eluent: THF): $M_n = 26.1 \text{ KD}$, $\text{PDI} = 2.2$.

Poly[2,5-bis(11-hydroxy-3,6,9-trioxaundecyl)-1,4-diethynyl-phenylene-*alt*-2,5-bis(11-(9'-anthracenecarboxylate)-3,6,9-trioxaundecyl)-1,4-phenylene] (PPE3, 530 mg, 95%) was synthesized following the same procedure as PPE2. $^1\text{H NMR}$ (300 MHz, CDCl_3 , δ/ppm): 3.53–3.65 (br, m, 44H), 3.83 (m, 10H), 4.06 (br, s, 6H), 4.74 (br, s, 4H), 7.04 (s, 4H), 7.39–7.48 (m, 8H), 7.98 (br, d, 4H), 8.10 (br, d, 4H), 8.47 (br, s, 2H). GPC (eluent: THF): $M_n = 20.5 \text{ KD}$, $\text{PDI} = 2.3$.

2.4. Preparation of Polymer/SWNTs Hybrids

As-prepared SWNTs were purified using a previously published method.¹⁹ The purified SWNTs were dispersed with the aid of a high power ultrasonic probe in chloroform (0.2 mg mL^{-1}) and were then blended with the polymer solution in chloroform (20 mg mL^{-1}) to make the SWNTs/PPE hybrid materials (mass ratio of SWNTs/polymer = 1/100, $C_{\text{polymer}} = 10 \text{ mg mL}^{-1}$) for device fabrication.

2.5. Photovoltaic Cell Fabrication

Photovoltaic devices were fabricated in the ITO/active layer/Al configuration (Fig. 1). The devices were fabricated on $2.5 \times 2.5 \text{ cm}^2$ ITO-coated glass substrates. The ITO was cleaned by ultrasonication and rinsed in deionized water, acetone, and *iso*-propanol. The active layer was formed by spin coating (1500 rpm) of a solution of 1 wt% of SWNTs in polymer from a 10 mg mL^{-1} chloroform solution prepared from the last section. Al electrode was deposited on the active layer by vacuum evaporation under $3 \times 10^{-4} \text{ Pa}$ and the thickness of which was controlled at $\sim 100 \text{ nm}$. Eight polymer solar cell devices were fabricated in one cut ITO glass, and the effective area of each cell is 4 mm^2 .

3. RESULTS AND DISCUSSION

3.1. Synthesis and Characterization of the Polymers

The synthetic routes of monomers and polymers are shown in Scheme 1 and the functionalized PPE polymers were prepared via Sonogashira crossing-coupling procedures. All polymers were rather soluble in common organic solvents such as chloroform, THF, dichloromethane, and toluene and good transparent films can be cast on glass substrates using these solutions. The average molecular weights were measured by gel permeation chromatography (GPC). The number average molecular weights (M_n) and the polydispersity indexes (PDI) are 9600 g mol^{-1} and 1.8,¹⁰ 26100 g mol^{-1} and 2.2, 20500 g mol^{-1} and 2.3 for PPE1, PPE2 and PPE3, respectively. As shown in Figure 2, all polymers exhibited an intense absorption band in CHCl_3 centered at $\sim 430 \text{ nm}$, which arises from the long axis polarized $\pi-\pi^*$ transition corresponding to the effective conjugation along the PPE backbone.¹⁵ The sword-like peaks of PPE3 arising from anthracene group of side chain broadens the absorption in the 350–500 nm band, which is expected to enhance the photovoltaic properties of PPE3 devices. The effective absorption range is below 320 nm for naphthalene. Thus, the naphthalene group on the side chain in polymer PPE2 does not have much impact of the polymer absorption spectrum compared with that of polymer PPE1 as seen in Figure 2. Considering the spectrum range of solar light ($>300 \text{ nm}$ range for AM 1.5), it is

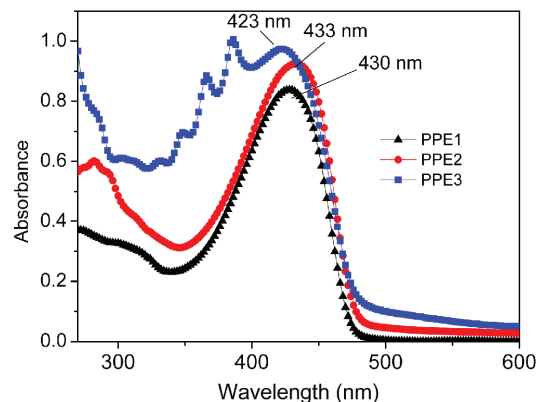


Fig. 2. UV-Vis absorption spectra of PPE1, PPE2 and PPE3 in CHCl_3 solution at a concentration of 0.02 mg mL^{-1} .

expected that this naphthalene group incorporation would not affect the overall solar light absorption of this material in the PV device.

The electrochemical behavior of the polymers is investigated by cyclic voltammetry (CV) in Figure 3, which is used to measure the redox potentials and evaluate the HOMO and LUMO energy level and the band gap energy of a polymer. The electrochemical processes are similar to the charge injection and transport in LED and photovoltaic devices. The CV experiments were carried out under the protection of argon with the solid film of the polymers cast on the platinum disk working electrode using their acetonitrile solution (10 mg mL^{-1}) at room temperature. The onset potentials are the values obtained from the intersection of the two tangents drawn at the rising current and the baseline charging current of the CV of the polymer curves.

In our experiment, the HOMO level for PPEs is estimated using the oxidation potential of the polymers whereas the LUMO energy is extrapolated from this value by using the optical band gap ($E_g^{\text{opt}} = 1240/\lambda_{\text{onset}}$) (Table I).²⁰ Thus, the HOMO and LUMO of polymers

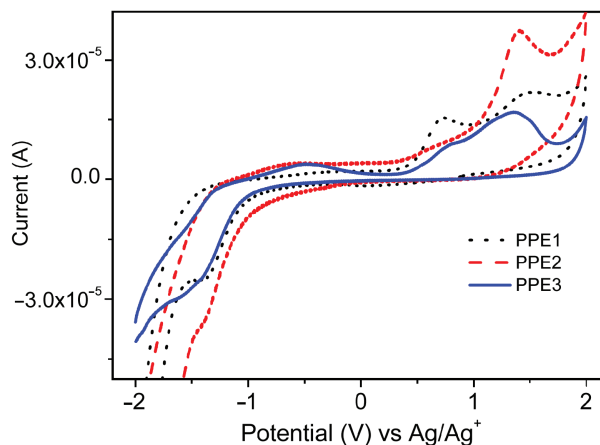


Fig. 3. Cyclic voltammograms of the PPE1, PPE2 and PPE3 films on a platinum electrode in 0.1 M TBAP acetonitrile solution.

Table I. Electrochemical onset potentials and electronic energy levels of the polymer films.

Polymer	$E_{\text{onset}}^{\text{ox}}$ (V vs. Ag/Ag ⁺)	λ_{onset} (nm)	$E_{\text{g}}^{\text{opt}}$ (eV)	HOMO (eV)	LUMO (eV)
PPE1	0.42	517	2.40	-5.15	-2.75
PPE2	0.40	508	2.41	-5.13	-2.72
PPE3	0.40	514	2.44	-5.13	-2.69

were estimated according to the following equation:²¹

$$\text{HOMO} = -e(E_{\text{onset}}^{\text{ox}} - E_{\text{Fc}/\text{Fc}^+} + 4.8) \text{ (eV)} \quad (2)$$

$$\text{LUMO} = \text{HOMO} - E_{\text{g}}^{\text{opt}} \text{ (eV)} \quad (3)$$

In which, $E_{\text{Fc}/\text{Fc}^+} = 0.07$ V versus Ag/Ag⁺. The results are summarized in Table I.

From Table I, we can see that all polymers exhibit very similar electronic energy levels, suggesting that there is little influence of the side group on the electronic properties of the PPE backbone. This conclusion is confirmed by that the absorbance spectra of PPE2 and PPE3 are almost superpositions of the spectra of PPE1 with their corresponding sensitizing groups.²²

3.2. SWNTs Characterization

High purity of donor or acceptor materials is in favor of the exciton and carrier diffusion, which will improve the photovoltaic properties. As-prepared SWNTs were purified using the hydrothermal method.¹⁹ Figure 4(a) shows a TEM image of purified SWNTs. No obvious amorphous carbon and carbon-encased metal catalyst were observed as shown in Figure 4(a) for a typical TEM image of purified SWNTs, indicating that the amount of impurities was largely removed after purification. SWNTs have a tendency to bundle together due to van der Waals interaction so that individual tubes are hardly to be seen in our samples. Figure 4(b) shows the Raman spectra of purified SWNTs. In the low-frequency region, there is a peak at ~ 173 cm⁻¹, assigned to the band of the radial breathing mode (RBM). According to the relationship between the RBM frequency with the tube diameter, $d = 234/(\omega - 10)$,¹⁷ the diameter of these Raman activated SWNTs with 514.5 nm laser is calculated to be 1.44 nm. Relative to the tangential mode at ~ 1596 cm⁻¹ (G-band), the intensity of the disorder mode at ~ 1345 cm⁻¹ (D-band) is very low, indicating the intact of SWNTs sidewall and high purity of the sample because D-band is related to the sp³ states of carbon.^{23,24}

3.3. Optical Properties

UV-Vis-NIR absorption spectra of all PPEs and their SWNTs blend composite cast films are shown in Figure 5. The PPE1 in CHCl₃ solution had an absorption peak around 430 nm (Fig. 2) whereas in the cast film absorption

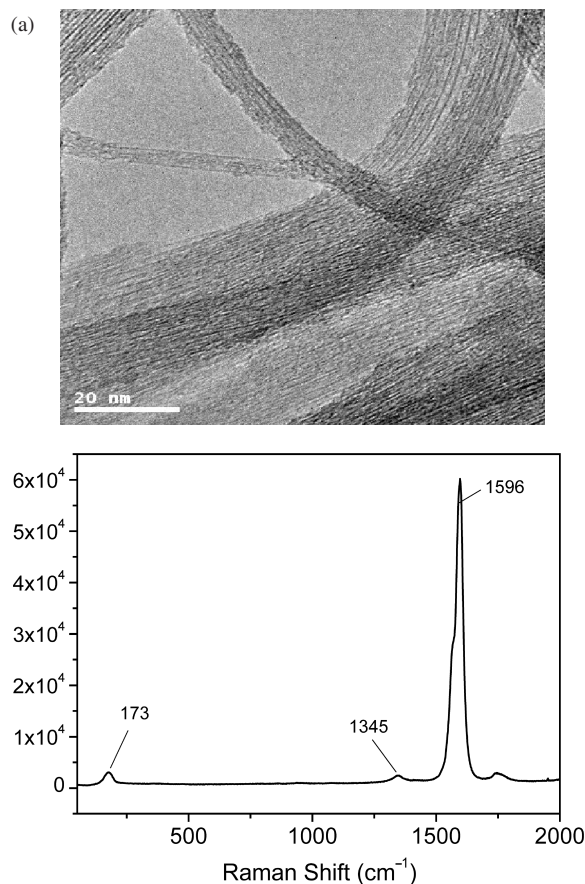


Fig. 4. (a) TEM image of purified SWNTs showing the bundle state and high purity. (b) Raman spectra (excited with 514.5 nm laser) of the purified SWNTs.

peak undergoes a 19 nm red shift, and a new shoulder absorption band around 490 nm arises due to the π - π stacking structure. For PPE2 and PPE3, 18 nm and 11 nm red shift were also observed for their cast films comparing with that of the polymer solution absorption respectively. In solid film, the planar shape of the conjugated polymer allows itself to easily arrange into a co-facial π - π stacking structure, resulting in a more coplanar conformation in film than in solution, hence enhancing the effective conjugation length. As a result, the position of the corresponding absorption peak is red shifted.²⁵

While the absorption spectra of PPEs film show no significant change upon adding 1 wt% of SWNTs. The typical absorbance of SWNTs, S₁₁ band at ~ 1800 nm and S₂₂ band at ~ 1000 nm (shown by arrows in the inset of Fig. 5), can still be discerned, indicating the unnegligible ingredient of SWNTs in the hybrids.

3.4. Photovoltaic Properties

3.4.1. The Influence of SWNTs Doping on the Photovoltaic Performance

The current-voltage (I - V) characteristics of ITO/active layer/Al devices in dark are shown in Figure 6. Forward

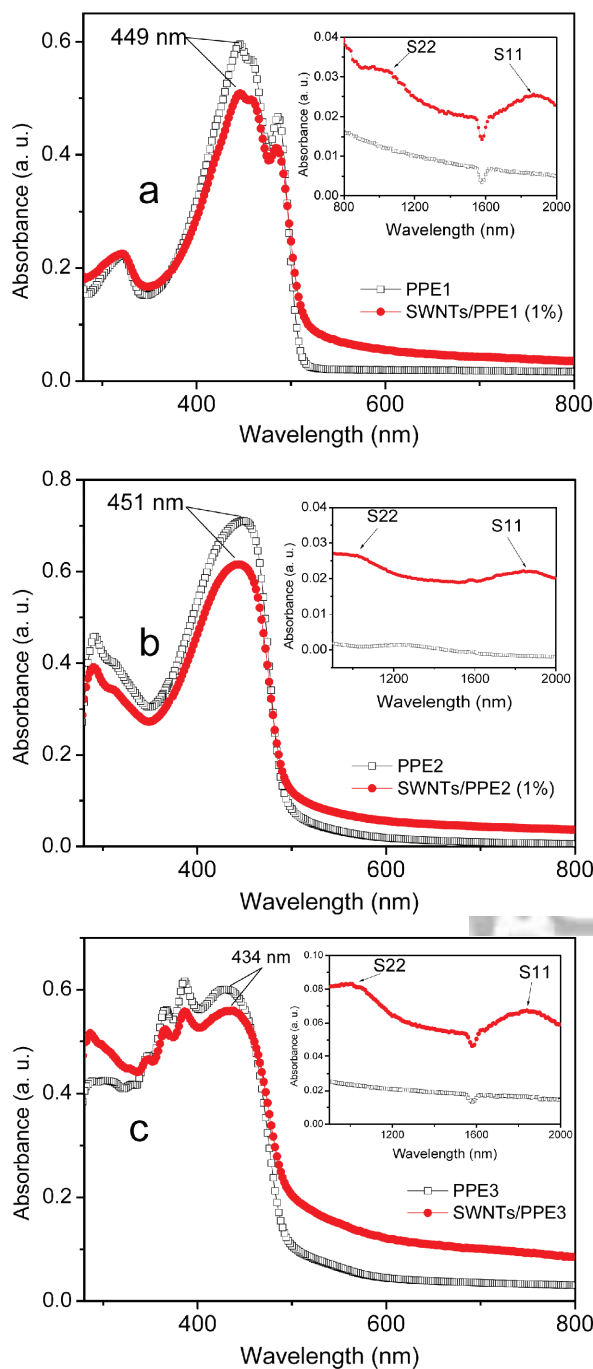


Fig. 5. UV-Vis-NIR absorption spectra of PPE1 film, SWNTs/PPE1 (1%) blend film (a), PPE2 film, SWNTs/PPE2 (1%) blend film (b) and PPE3 film, SWNTs/PPE3 (1%) blend film (c) on quartz substrates taken in transmission mode.

bias is defined as positive voltage applied to the ITO electrode. The dark currents are higher in forward bias than in reverse bias, indicating the diode behavior. The dark currents significantly increased after adding SWNTs into the polymer matrix, suggesting that the conductivity of the devices increased by incorporating SWNTs into the system.

Under illumination, as shown in Figure 7 and Table II, the V_{oc} of pristine polymers device exhibit the similar

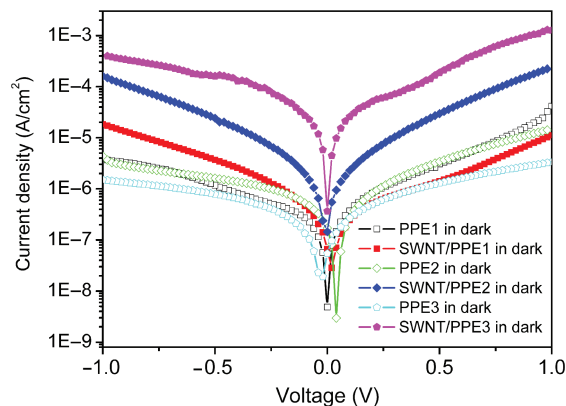


Fig. 6. I - V characteristics of the polymer solar cells based on PPEs and SWNTs/PPEs hybrids (1%) in dark.

value (~ 0.4 V). According to metal-insulator-metal (MIM) diode model for the pure polymer systems,²⁶ the V_{oc} is determined by the work function difference of the two electrodes. The work function of Al is 4.3 eV, and the work function of ITO is 4.7 eV.²⁷ Thus, the upper limit of the V_{oc} should be around 0.4 V, which is the value we got for our pure PPE systems without SWNT hybridizing.

Whereas, the V_{oc} (0.44 V) of SWNTs/PPE3 device is higher than the upper limit of the theoretic V_{oc} according to MIM model. For bulk heterojunction devices, Fermi energy pinning mechanism has been successfully used for explanation of the V_{oc} of SWNTs/P3OT photovoltaic device by Kymakis et al.⁸ They found that the work function of the metal has no significant effect on the V_{oc} , and the upper limit of the V_{oc} is determined by the difference of the P3OT HOMO and the SWNTs work function. It is known that the Fermi level of the negative electrode is "pinned" to the reduction potential of the fullerene in bulk-heterojunction devices made out of donor polymers and acceptor fullerenes.²⁶ Fermi level pinning describe a situation where the work function of electrode is pinned to the work function of the semiconductor. This occurs independently whether the metal work function is higher

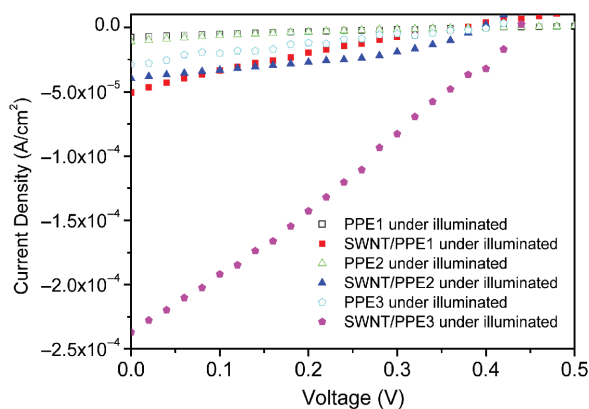


Fig. 7. I - V curves of the polymer solar cells as a liner plot based on PPE1, PPE2, PPE3 and SWNTs/PPE1, SWNTs/PPE2, SWNTs/PPE3 hybrids (1%) under the illumination of AM1.5, 100 mW cm^{-2} .

Table II. Properties of ITO/active layer/Al photovoltaic cells.

Active layer	V_{oc} (V)	I_{sc} ($\mu\text{A cm}^{-2}$)	FF	η (%)
PPE1	0.40	7.4	0.21	6.5×10^{-4}
PPE2	0.38	10.9	0.21	8.3×10^{-4}
PPE3	0.40	28.9	0.23	2.7×10^{-3}
SWNTs/PPE1	0.36	50.6	0.22	4.2×10^{-3}
SWNTs/PPE2	0.40	39.5	0.39	6.2×10^{-3}
SWNTs/PPE3	0.44	237	0.30	0.031

or lower than the semiconductor Fermi level. This results in a V_{oc} that is directly related to the energy difference between the HOMO level of the donor and the LUMO level of the acceptor material. Thus, varying the difference in work function between positive and negative electrode in these devices has only minor effects on the V_{oc} .

In our experiment, the HOMO of our polymer is ~ 5.1 eV according to the electrochemical results. If SWNTs work function is taken as 4.6 eV,²⁸ the maximum expected V_{oc} of polymers would be around 0.5 V, which are consist with our experimental results. Though the work function of SWNTs will change with the chirality and diameter, usually the work function of metallic SWNTs is in the range of 4.63–4.77 eV, and the work function of semiconducting SWNTs has a larger value than that of metallic SWNTs.²⁸

The I_{sc} are very different for the devices, the light current is significantly increased after SWNTs doping, as shown in Figure 7 and Table II. This increased current of hybrid device comparing with the current of pristine polymer device is believed due to the introduction of SWNTs into the polymer matrix by forming SWNTs/polymer bulk heterojunction.⁷ These junctions act as dissociation centers, which are able to split up the exciton into free charges and also create a continuous pathway for charges to be transported to the electrodes.

All the power conversion efficiency of devices of SWNTs/PPE is also enhanced ~ 1 order magnitude than that of their corresponding pristine polymer devices. The better performance of SWNTs/PPE devices than that of PPE devices clearly indicate that SWNT incorporation into the hybrids significantly improve the exciton generation and charge separation due to the intrinsic bulk heterojunction between SWNTs and PPEs.

3.4.2. The Influence of the Polymer Side Chain on the Photovoltaic Performance

As shown in Table II, the I_{sc} of SWNTs/PPE3 device ($237 \mu\text{A cm}^{-2}$) is remarkably higher than that of SWNTs/PPE1 ($50.6 \mu\text{A cm}^{-2}$) and SWNTs/PPE2 ($39.5 \mu\text{A cm}^{-2}$) devices and similar trend is found for the bare PPE3 ($28.9 \mu\text{A cm}^{-2}$), PPE2 ($10.9 \mu\text{A cm}^{-2}$) and PPE1 ($7.4 \mu\text{A cm}^{-2}$) devices.

The FF of the device with anthracene sensitizer is also improved from 0.22 to 0.30 comparing the SWNTs/PPE1

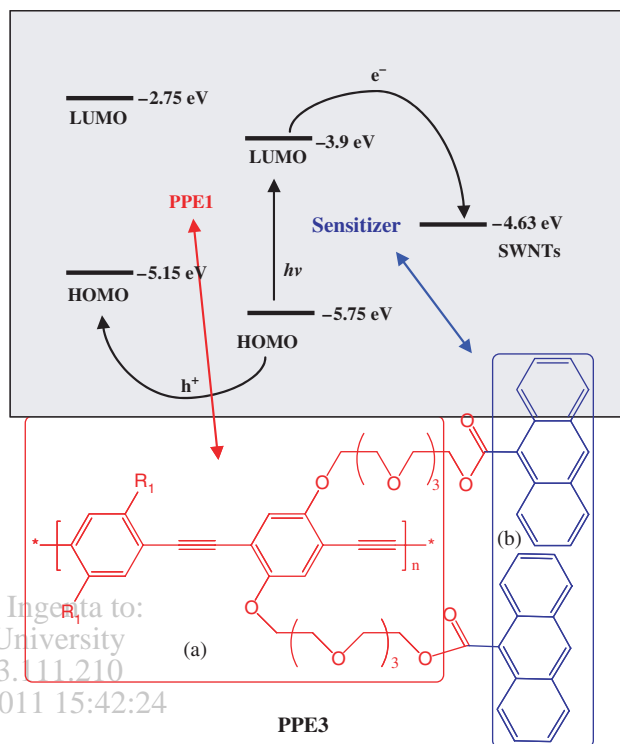


Fig. 8. Schematic diagram of energy levels for PPE3 segment (a), anthracene (b), and SWNTs relative to vacuum level shows the proposed energetically possible charge-transfer process from photoexcited anthracene group to PPE3 backbone and SWNTs.

device with SWNTs/PPE3 device. For SWNTs/PPE2 device, the FF is ~ 0.39 which is significantly higher than that of SWNTs/PPE1 and SWNTs/PPE3 devices. This increase may be due to the longest average backbone of PPE2 comparing with that of PPE1 and PPE3. The degree of polymerization (DP) is ~ 22 , ~ 20 and ~ 15 for PPE1, PPE2 and PPE3 respectively, indicating ~ 15 nm average backbone length for PPE1, ~ 27 nm backbone for PPE2 and ~ 20 nm backbone for PPE3. While we do not understand the exact mechanism why PPE2 device has significantly increased fill factor, the increased relatively longer backbone of PPE2 may result in a more efficient heterojunction formation and better channel for the dissociated charges.

The power conversion efficiency of device SWNTs/PPE1 and SWNTs/PPE2 is $4.2 \times 10^{-3}\%$ and $6.2 \times 10^{-3}\%$, respectively. While for SWNTs/PPE3 device, the power conversion efficiency is enhanced to 0.031%, which is comparable to previous reports of SWNTs/polythiophene device by Kymakis et al.^{7,8}

Comparing PPE1 and PPE2 with PPE3, the anthracene group as the sensitizer bonded on PPE3 side chain broaden the absorption in the 350–500 nm bands, which may be the most important reason of the enhancement of the device PV performance. Photoexcited charge transfer of anthracene group at the polymer/nanotube interface is expected to take place, and this process is known

as sensitization.²⁹ The possible energy levels diagram for sensitization induced charge-transfer process is shown in Figure 8. The energies of LUMO and HOMO of anthracene group (b, shown in Fig. 8) in PPE3 are assumed to be equal to that of a similar molecule anthracene.³⁰ Energy levels of PPE3 without anthracene group on the side chains (a, shown in Fig. 8) are assumed the same to that of PPE1 because there is little influence of the side group on the electronic properties of the PPE backbone. Thus, the photoexcited anthracene transfer an electron to the nanotube, and a hole is transferred to the high lying HOMO of PPE backbone, then the carriers were transferred to the electrodes forming electrical current. The I_{sc} of PPE3 backbone can be assumed equal to I_{sc} of PPE1, then I_{sc} of sensitizer molecule is equal to $I_{sc(PPE3)} - I_{sc(PPE1)}$. With this assumption, the photocurrent component from the photoexcited PPE3 backbone ($50.6 \mu\text{A cm}^{-2}$) is only about 1/4 of the current value from the sensitizer molecule ($237 - 50.6 \mu\text{A cm}^{-2}$). Therefore, sensitization of anthracene group in this system is the main origin of the much enhanced photocurrent. These results suggest that we can improve the properties of PSC by proper sensitizer molecule modification of the polymer, giving a new way to design high efficiency PSC.

4. CONCLUSIONS

In summary, a novel PPE/SWNTs donor-acceptor system is constructed and the system exhibits improved photovoltaic properties comparing with pristine PSC. SWNTs in the donor-acceptor system play an important role in better dissociating excitons into electrons and holes and transporting electrons to electrodes. By bonding anthracene group on the polymer (PPE3) side chain, the photovoltaic properties of SWNTs/PPE3 device ($I_{sc} = 237 \mu\text{A cm}^{-2}$, $V_{oc} = 0.44$, $\eta = 0.031\%$) are significantly improved comparing with that of SWNTs/PPE1 ($I_{sc} = 50.6 \mu\text{A cm}^{-2}$, $V_{oc} = 0.36$, $\eta = 4.2 \times 10^{-3}\%$) and SWNTs/PPE2 ($I_{sc} = 39.5 \mu\text{A cm}^{-2}$, $V_{oc} = 0.40$, $\eta = 6.2 \times 10^{-3}\%$) devices. The improvement of the device performance comes from the sensitization of anthracene group, which gives a new way to design high performance PSC.

Acknowledgments: The authors gratefully acknowledge the financial support from MoST (#2006CB932702), MoE (#20040055020), the NSF (#20644004 and 60676051) of China and the NSF (#07JCYBJC03000 and 06TXTJJC14603) of Tianjin City.

References and Notes

1. J. M. Halls, C. A. Walsh, N. C. Greenham, E. A. Marseglia, R. H. Friend, S. C. Moratti, and A. B. Holmes, *Nature* 376, 498 (1995).
2. G. Yu, J. Gao, J. C. Hummelen, F. Wudl, and A. J. Heeger, *Science* 270, 1789 (1995).
3. N. S. Sariciftci, L. Smilowitz, A. J. Heeger, and F. Wudl, *Science* 258, 1474 (1992).
4. M. Grantstorm, K. Petritsch, A. C. Arias, A. Lux, M. R. Andersson, and R. H. Friend, *Nature* 395, 257 (1998).
5. S. Gunes, H. Neugebauer, and N. S. Sariciftci, *Chem. Rev.* 107, 1324 (2007).
6. C. J. Brabec, N. S. Sariciftci, and J. C. Hummelen, *Adv. Funct. Mater.* 11, 15 (2001).
7. E. Kymakis and G. A. J. Amaratunga, *Appl. Phys. Lett.* 80, 112 (2002).
8. E. Kymakis, I. Alexandrou, and G. A. J. Amaratunga, *J. App. Phys.* 93, 1764 (2003).
9. S. Bhattacharyya, E. Kymakis, and G. A. J. Amaratunga, *Chem. Mater.* 16, 4819 (2004).
10. J. Mao, Q. Liu, X. Lv, Z. Liu, Y. Huang, Y. Ma, Y. Chen, and S. Yin, *J. Nanosci. Nanotechnol.* 7, 2709 (2007).
11. J. X. Geng and T. Y. Zeng, *J. Am. Chem. Soc.* 128, 16827 (2006).
12. J. A. Rud, L. S. Lovell, J. W. Senn, Q. Q. Qiao, and J. T. Mcleskey, *J. Mater. Sci.* 40, 1455 (2005).
13. E. Kymakis, E. Koudoumas, I. Franghiadakis, and G. A. J. Amaratunga, *J. Phys. D: Appl. Phys.* 39, 1058 (2006).
14. B. J. Landi, R. P. Ruffaelle, S. L. Castro, and S. G. Bailey, *Prog. Photovolt: Res. Appl.* 13, 165 (2005).
15. U. H. F. Bunz, *Chem. Rev.* 100, 1605 (2000).
16. J. Chen, H. Y. Liu, W. A. Weimer, M. D. Halls, D. H. Waldeck, and G. C. Walker, *J. Am. Chem. Soc.* 124, 9034 (2002).
17. X. Lv, F. Du, Y. F. Ma, Q. Wu, and Y. S. Chen, *Carbon* 43, 2020 (2005).
18. D. C. Lee, B. J. Chang, G. M. Morales, Y. A. Jang, M. K. Ng, S. T. Heller, and L. P. Yu, *Macromolecules* 37, 1849 (2004).
19. K. Tohji, T. Goto, H. Takahashi, Y. Shinoda, N. Shimizu, B. Jeyadevan, I. Matsuoka, Y. Saito, A. Kasuya, T. Ohsuna, K. Hiraga, and Y. Nishima, *Nature* 383, 679 (1996).
20. J. K. Mwaura, M. R. Pinto, D. Witker, N. Ananthkrishnan, K. S. Schanze, and J. R. Reynolds, *Langmuir* 21, 10119 (2005).
21. Q. J. Sun, H. Q. Wang, C. H. Yang, and Y. F. Li, *J. Mater. Chem.* 13, 800 (2003).
22. A. R. A. Palmans, P. Smith, and C. Weder, *Macromolecules* 32, 4677 (1999).
23. H. Q. Peng, L. B. Alemany, J. L. Margrave, and V. N. Khabashesku, *J. Am. Chem. Soc.* 125, 15174 (2003).
24. M. S. Dresselhaus, G. Dresselhaus, A. Jorio, A. G. Souza, and R. Saito, *Carbon* 40, 2043 (2002).
25. U. H. F. Bunz, J. M. Imhof, R. K. Bly, C. G. Bangcuyo, L. Rozanski, and D. A. V. Bout, *Macromolecules* 38, 5892 (2005).
26. M. C. Scharber, D. Wuhlbacher, M. Koppe, P. Denk, C. Waldauf, A. J. Heeger, and C. L. Brabec, *Adv. Mater.* 18, 789 (2006).
27. I. D. Parker, *J. App. Phys.* 75, 1656 (1993).
28. J. J. Zhao, J. Han, and J. P. Lu, *Phys. Rev. B* 65, 193401 (2002).
29. B. O'regan and M. Grätzel, *Nature* 353, 737 (1991).
30. M. Pope and C. E. Swenberg, *Electronic Processes in Organic Crystals and Polymers*, 2nd edn., Oxford University Press, New York (1999).

Received: 6 June 2007. Accepted: 19 September 2007.